



ELSEVIER

Microelectronic Engineering 61–62 (2002) 693–699

**MICROELECTRONIC  
ENGINEERING**

www.elsevier.com/locate/mee

# The role of secondary electrons in electron-beam-induced-deposition spatial resolution

N. Silvis-Cividjian\*, C.W. Hagen, L.H.A. Leunissen, P. Kruit

*Department of Applied Physics, Delft University of Technology, Lorentzweg 1, 2628 CJ Delft, The Netherlands*

---

## Abstract

Electron-beam-induced-deposition (EBID) is a versatile direct writing technique occasionally used in micro- and nanofabrication. We focus in our study on the EBID spatial resolution, defined as the lateral size of the smallest deposited structure. The lateral size of dot structures always exceeds the diameter of the electron probe. Many authors have argued that this is due to the secondary electrons emitted as a result of primary electron bombardment, but it has never been modeled quantitatively. We developed a model based on Monte Carlo methods that simulates the role of secondary electrons in the spatial evolution of EBID dots. The results show that the secondary electrons are indeed responsible for the shapes and sizes observed during EBID. The secondary electrons generated inside the substrate by a pin-point primary beam produce initially a very small structure broadening, of about one nanometer. Then using a dynamic Monte Carlo profile simulator which includes the electron scattering in the already grown tip structure, we show for the first time that the laterally emerging secondary electrons are continuously enlarging the tip diameter, up to saturation values of 20–30 nm, in agreement with experiments. © 2002 Elsevier Science B.V. All rights reserved.

*Keywords:* Electron-beam-induced-deposition; Spatial resolution; Secondary electrons; Monte Carlo simulations; Profile simulator

---

## 1. Introduction

Electron-beam-induced-deposition (EBID) allows fabrication of three-dimensional nanometer-sized structures on targets of different geometries [1]. The process is not fully understood, but the basic principle can be described as follows. A substrate coated with adsorbed precursor molecules is exposed to a focused electron beam. As a result of complex beam-induced reactions, the precursor molecules dissociate into deposited material and volatile fragments, which are pumped out. Depending on the precursor, the deposit consists of metal atoms, carbon atoms, or nanocrystals embedded in a matrix of amorphous carbon.

---

\*Corresponding author.

The spatial resolution of EBID is determined by many factors, like the electron transport to the surface, the parameters of the gaseous precursor, the target and its environment, various surface processes, delocalization effects, etc. When studying the role of the electrons on EBID, most existing models consider only the parameters of the primary electron beam [2,3]. However, there is abundant experimental evidence that the lateral size of dots and lines, fabricated by EBID, considerably exceeds the diameter of the electron beam writing tool [4–6]. For example the best result today is a linewidth of 13 nm deposited with a 2-nm beam diameter [7]. According to many authors, this lateral broadening is mainly caused by the low energy secondary electrons, emitted from the substrate as a result of the primary electron beam irradiation [8]. This assumption is based on the fact that the cross-section for electron-impact molecular dissociation, the main process in EBID, peaks at low electron kinetic energies. However, a complete theoretical model that explains this lateral broadening has not been issued yet. The objective of this article is to fill this gap and quantify the role of the secondary electrons in determining the spatial resolution of EBID. Results are presented of Monte Carlo simulations for secondary electron emission and for the growth of the deposit, which are well in agreement with experimental observations.

## 2. The model

Consider a typical EBID process in which a finely focused electron beam is kept stationary on a target covered by precursor molecules. After a short time, a conical structure starts to grow on the target, localized in the electron irradiated area. This is also well-known from contamination growth in electron microscopes. The diameter of the cone, measured at its base or at half maximum height, initially grows steeply and after some time reaches a saturation value which always exceeds the diameter of the electron probe at the target. Typically encountered values range from 20 to 500 nm for beam diameters of 2–10 nm on both thin and bulk specimens [4–6,9]. The exact time behaviour of the diameter is hard to give, as it depends on many parameters like the settings of the electron optics, the partial pressure of the precursor gas, the surface diffusion of the precursor molecules, the cleanliness of the specimen, etc. But qualitatively the diameter versus time curve will be as sketched in Fig. 1, in which the following regimes can be distinguished: the nucleation stage (marked 0–A in Fig. 1) when no significant growth is observed, an intermediate regime (A–B) characterized by a fast growth of the

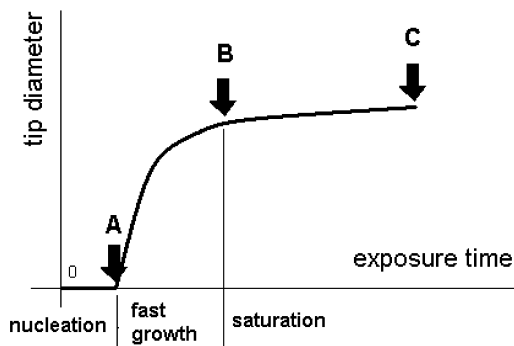


Fig. 1. A typical curve showing the evolution of the cone diameter.

structure diameter, and the saturation regime (B–C) where the diameter attains a more or less constant value.

This behaviour can be modeled as follows. After some time following the start of the electron beam exposure, the nucleation is completed (point A in Fig. 1). The primary electrons (PE) hit the flat substrate surface and generate secondary electrons (SE) in the substrate which are partly emitted from the flat substrate, from an area larger than the beam diameter. Both types of electrons, PE and SE, will dissociate the adsorbed molecules and a dot will start to be deposited, its diameter being determined by the exit area of SE on the target surface. Although this scenario has been brought up by many authors as an explanation for the growth of structures broader than the primary beam size, we will show from Monte Carlo simulations that experimentally observed structure sizes cannot be explained this way at all. Therefore we extended this model by including scattering in the freshly grown structure also. To our knowledge this has never been done before and we will show the importance of this. While the tip-like structure grows in vertical direction, the PE entering the apex of the tip may scatter in the tip, generating SE that can exit the tip from its side walls. These secondary electrons will dissociate the precursor molecules adsorbed on the tip flanks and thus will contribute to an extra lateral broadening. Saturation will occur when the secondary electrons will not be able to exit the side flanks anymore. This moment will be determined by the escape depth, i.e., the inelastic mean free path, of the secondary electrons in the deposit (5–15 nm) [10].

The spatial profile of the deposit is thus determined by secondary electrons generated and propagating in two different materials. Initially by the SE emitted from the flat substrate and later by the SE emitted from the side flanks of the deposited tip. If we define the EBID resolution as the smallest lateral structure size that can be deposited, then the ultimate resolution will be obtained at point A in Fig. 1. This will be achieved only for very small primary beam diameter. A more realistic lateral resolution, which can be routinely achieved, will be obtained at point B in Fig. 1. In the following sections we will investigate the role the secondary electrons play at these two moments A and B and we will prove the validity of our model.

### 3. The role of secondary electrons emitted from a flat target substrate

The growth rate in each point on the substrate surface,  $R(x)$  is given by [11]:

$$R(x) = \int_0^{E_0} f(x,E) \sigma_{\text{diss}}(E) N \, dE$$

(in no. of molecules/unit area/s) where  $f(x,E)$  (in no./unit area per s) is the flux of electrons, PE and SE, passing through the surface as a function of position and energy,  $\sigma_{\text{diss}}(E)$  (unit area) is the electron-induced dissociation cross-section of the precursor molecule as function of incident electron kinetic energy  $E$  and  $N$  (no./unit area) is the surface density of adsorbed precursor molecules. The flux of PE,  $f_{\text{PE}}(x,E)$ , is easily calculated assuming that the beam is monochromatic and the current distribution at the surface is a Gaussian. The flux of SE emitted from the surface,  $f_{\text{SE}}(x,E)$ , can be estimated using simulations of electron scattering in a solid target. Such simulations can be performed for a zero-diameter electron beam using the Monte Carlo method and have been successfully applied,

throughout the years, to imaging analysis in scanning electron microscopy (SEM) and resist-based electron beam lithography (EBL) [12].

We developed a new Monte Carlo simulation program for electron-induced secondary emission customized for the ultimate EBID resolution study, i.e., thin substrates and high kinetic energies. Thinner substrates (5–100 nm) display less scattering and therefore the exit area of the secondary electrons is expected to be smallest. To be able to achieve the best fabrication resolution one has to use scanning transmission electron microscopes (STEM) which have the smallest possible primary beam size. Therefore the simulations have to deal with high kinetic energies (100–300 keV). The program is written as a Windows application in a Delphi programming environment. The output data contains the exit radial position and the energy of the secondary electrons, in contrast with simulations on SEM imaging analysis, where only the cumulative energy spectrum is of interest.

The elastic scattering has been treated using the Rutherford cross-section. The electron inelastic scattering has been treated using the fast secondary electrons model proposed by Joy [12]. The detailed description of the simulation model will be the subject of a separate article. To calculate the deposition rate the cross-section for electron-induced chemistry,  $\sigma_{\text{diss}}(E)$ , has to be determined. Unfortunately this kind of data is nearly complete only for a few gases present in the atmosphere and interstellar spaces ( $\text{H}_2$ ,  $\text{N}_2$ ,  $\text{CO}$ ,  $\text{CH}_4$ ), and gases used in plasma-assisted micromachining ( $\text{CF}_4$ ). Because of this lack of information, many authors have used simplified models [2,12,13]. We have used an accurate dissociation cross-section dependence on electron energy for the  $\text{C}_2\text{H}_5$  hydrocarbon precursor [14].

As a numerical example we consider the case of carbon growth on a 5 nm thin copper target using a zero-diameter 20 kV primary beam. In Fig. 2 the normalized deposition rate  $R(x)$  due to EBID by SE from the flat substrate is shown as function of radial position measured from the point of PE incidence (solid line). The full width at half maximum (FWHM) is 0.4 nm. A better measure of the size of the deposit is obtained by determining the radius within which 50% of the deposited atoms are contained (FW50%). This value is 1.2 nm as can be read from the normalized integral function of the radial distribution of deposited atoms  $N_{\text{tot}}(x)$  (dashed line). A convolution between this result and a typical Gaussian primary beam of 2 nm diameter gives an EBID resolution (at point A in Fig. 1) of 2.5 nm.

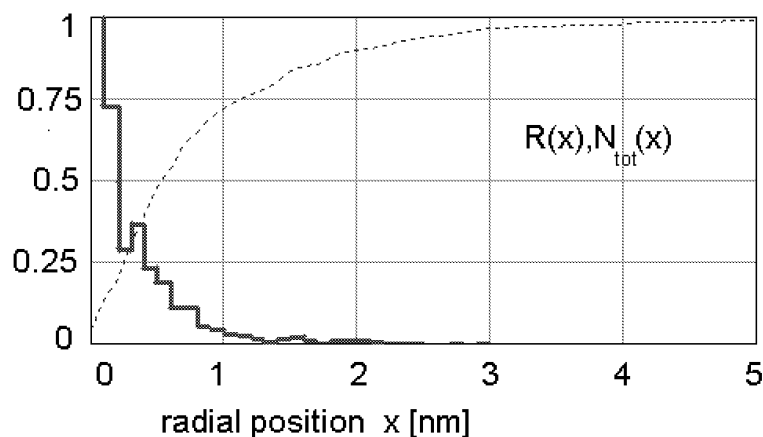


Fig. 2. The normalized deposition rate  $R(x)$  (solid line) determined by the SE from the flat substrate (no. atoms/ $\text{nm}^2$  per s), and the normalized integral function of the radial distribution of the deposited atoms  $N_{\text{tot}}(x)$  (no. atoms/nm) (dashed line).

However, the smallest experimentally observed features deposited with a 2 nm primary beam are typically 15–20 nm [6,7]. This discrepancy motivates to continue the simulations for deposition times later than point A in Fig. 1. To this purpose the next section describes a profile simulator for the deposited tip. The Monte Carlo simulations are extended with a dynamical update of the shape of the deposited structure each time a PE scattering is terminated.

#### 4. The role of secondary electrons emitted from the tip structure

We consider a simplified case, in which carbon is grown on a thin carbon foil, in order to avoid complicated interface effects. This situation, with an almost zero-diameter electron beam at high acceleration voltage (100–300 kV) is typical for high-resolution contamination growth on a carbon film and the simulation results can be easily checked against experiments in a modern STEM.

Because the amount of calculations increases drastically, a simple model has been adopted for the electron scattering simulation, that neglects the PE elastic scattering and applies the straight line approximation model for the secondary electrons, earlier proposed by Chung and Everhart [15]. An exponential decay of SE energy is assumed, using the inelastic mean free path given by Seah and Dench [16]. The profile simulator is based on a cellular automata method. The cylindrical symmetry of the deposit allows to replace its three-dimensional volume by a two-dimensional slice, normal to the substrate, containing the beam axis. Each discrete cell in the mesh is  $0.5 \times 0.5$  nm and can be in three states: ‘occupied’, ‘border cell’ or ‘unoccupied’. Each SE accumulates energy in the border cell of its exit position. When a PE simulation is finished, each border cell is inspected and if its normalized energy exceeds a threshold value (4 eV) then the molecule dissociates and a fragment is pinned. The cell state changes to ‘occupied’ and its neighbours become new border cells. The border is updated and the simulation process continues with another PE.

In Fig. 3 a time sequence of deposited dot profiles is shown. It is clearly seen that the dot diameter grows steadily from a few nanometers to approximately 20 nm (FWHM). Only at the very beginning of the deposition process the structure size can be very small, but soon after that, the structure grows laterally to sizes which are usually observed in experiments. The shapes and the deposits on the bottom side of the thin foil agree with electron microscopy contamination experiments.

#### 5. Conclusions

A model was presented to explain the shape and the lateral size of tips, experimentally grown using EBID in spot mode of an electron microscope. The model confirms the major role played by the secondary electrons emitted under electron beam irradiation. The secondary electrons emitted from the substrate surface play a key role in the very beginning of the growth process and establish the ‘theoretical’ ultimate EBID resolution at around 1 nm. To build such small structures is quite a challenge because they are also very thin, making the visualization difficult and ambiguous in a SEM or a STEM system. What happens after the very beginning has for the first time been successfully modeled by taking into account the electron scattering in the grown structure. This leads to a broadening of the structures caused by secondary electrons generated in the deposit dissociating adsorbed molecules on the side flanks of the deposit. This broadening is in agreement with

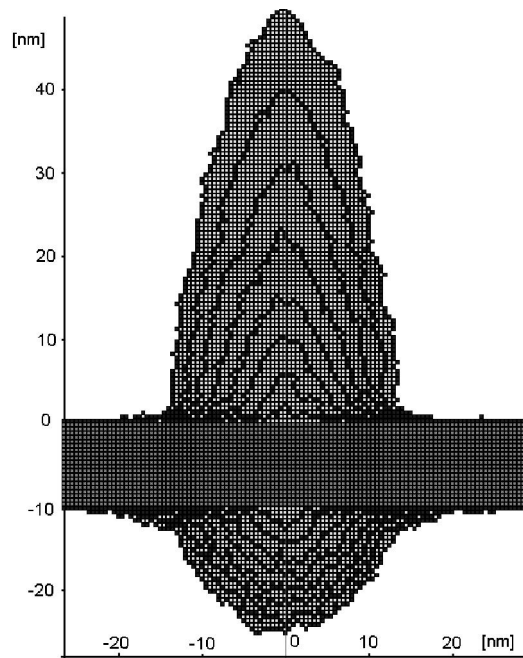


Fig. 3. A sequence of simulated profiles of a contamination tip grown by a 200-keV, zero diameter, electron beam on a 10-nm carbon foil, in steps of 9000 PE, starting at 3000 PE.

experimental observations. Visible tips have already diameters of 10–30 nm even for a zero-diameter primary beam. Because of similarities between EBID and specimen contamination in electron microscopes, the proposed model can be also very useful for high-resolution electron microscopy.

### Acknowledgements

This work is part of the research program of the ‘Stichting voor Fundamenteel Onderzoek der Materie’ (FOM), which is supported financially by the ‘Nederlandse Organisatie voor Wetenschappelijk Onderzoek’ (NWO).

### References

- [1] H.W.P. Koops, *J. Vac. Sci. Technol.* B6 (1988) 477.
- [2] H.W.P. Koops, *J. Vac. Sci. Technol.* B13 (1995) 2400.
- [3] V. Scheuer, *Microel. Eng.* 5 (1986) 423.
- [4] K.T. Kohlmann, *J. Vac. Sci. Technol.* B11 (1993) 2219.
- [5] K.I. Schiffmann, *Nanotechnology* 4 (1993) 163.
- [6] U. Hubner, R. Plontke, M. Blume, A. Reinhardt, H.W.P. Koops, *Microel. Eng.* 57/58 (2001) 953.
- [7] M. Komuro, H. Hiroshima, *Microel. Eng.* 35 (1997) 273.
- [8] P.C. Hoyle, J.R. Cleaver, H. Ahmed, *J. Vac. Sci. Technol.* B14 (1996) 662.

- [9] V. Harada, T. Tomita, T. Watabe, H. Watanabe, T. Etoh, *Scan. Electron Microsc. II* (1979) 105.
- [10] L. Reimer, in: *Scanning Electron Microscopy*, Springer, Berlin, 1998.
- [11] T.E. Allen, R.R. Kunz, T.M. Mayer, *J. Vac. Sci. Technol. B6* (1988) 2057.
- [12] D.C. Joy, in: *MC Modeling for Electron Microscopy and Microanalysis*, Oxford University Press, London, 1994.
- [13] P.W.H. de Jager, thesis, Delft, 1997.
- [14] D.A. Alman, D.N. Ruzic, J.N. Brooks, *Phys. Plasmas* 7 (2000) 1421.
- [15] M.S. Chung, T.E. Everhart, *J. Appl. Phys.* 45 (1973) 707.
- [16] M.P. Seah, W.A. Dench, *Surf. Interf. Anal.* 1 (1979) 2.